Trifluoroacetic Acid; r_0-Structure, Partial Substitution Structure and Deuterium Nuclear Quadrupole Coupling Studied by Molecular Beam Microwave Fourier Transform Spectroscopy and by *ab initio* Calculations

S. Antolinez, J. L. Alonso, H. Dreizler[a], E. Hentrop[a], and D. H. Sutter[a]

Departamento de Quimica Fisica, Facultad de Ciencias, Universidad de Valladolid, 47005 Valladolid, Spain

[a] Institut für Physikalische Chemie, Universität Kiel, Olshausenstr. 40, D-24098 Kiel

Reprint requests to Prof. D. H. S.; e-mail: sutter@phc.uni-kiel.de

Z. Naturforsch. **54 a,** 524–538 (1999); received August 3, 1999

Dedicated to Prof. Dr. H. D. Rudolph, Ulm, on occasion of his 75th birthday

We report the assignment and analysis of all stable monosubstituted isotopomers of trifluoroacetic acid. The ^{13}C and ^{18}O isotopomers were observed in natural abundance. The rotational constants and quartic centrifugal constants are presented. The rotational constants are used to derive a partial substitution structure and a complete r_0 structure for future comparison with the corresponding values in hydrogen bridged bimolecules containing trifluoroacetic acid as a subunit. The deuterium nuclear quadrupole coupling constants are derived from the hfs-splittings of low-J rotational transitions of the CF_3COOD isotopomer. The results of ab initio quantum chemical calculations are presented, which were carried out to assist in the assignment of the rotational spectra of the isotopomers and for comparison with the experimental molecular parameters.

Key words: Microwave Spectroscopy; Structure; D-hfs; Vibrational Averaging; *ab initio* Calculations.

1. Introduction

Trifluoroacetic acid, CF_3COOH, is one ligand in a series of hydrogen bridge bonded bimolecules, which have been investigated with microwave spectroscopy in the pioneering studies by Costain and Srivastava [1, 2] in the early sixties and by Bellot and Wilson [3] in the mid seventies. Recently it was demonstrated that molecular beam Fourier transform microwave spectroscopy (MBFTMW) can be applied to obtain more detailed information on such bimolecules. In these studies the second ligands were formic acid, HCOOH, and acetic acid, CH_3COOH, [4] and cyclopropane carboxylic acid, C_3H_5COOH, [5]. Our latter study initiated the present work, since only a preliminary experimental structure, based on electron diffraction data and on the rotational constants of CF_3COOH and of CF_3COOD, was available until now. Accurate structures of the free monomer subunits are of interest for instance, if one wants to study structural changes which occur upon complex formation.

One of the most efficient experimental methods to determine accurate structures for small molecules is MBFTMW spectroscopy. Over the past years this technique has matured so far that it is now capable to provide information with better than ppm accuracy on the rotational constants of most monosubstituted isotopomers of a compound *in natural abundance*, i. e. without the necessity to go through sometimes difficult, time consuming and possibly expensive chemical preparations. The structure is then derived by well established methods [6] from the observed rotational constants, see below.

The microwave spectra of CF_3COOH and of CF_3COOD have been investigated earlier by Stolwijk and van Eijck [7]. Their analysis was based on the electron diffraction structure [8]. Only the r_s-coordinate of the hydrogen atom has been given by these authors to demonstrate that the OH bond is cis to the C = O bond. In the following we present a complete microwave structure, based on highly accurate rotational constants for the most abundant species, the deuterated species and the monosubstituted ^{13}C and ^{18}O isotopomers. A more complete determination of the structure of the second ligand in the complex studied in [5], i. e. of cyclo-

0932–0784 / 99 / 0800–0524 $ 06.00

propane carboxylic acid, is in progress at our laboratory.

It should be mentioned that the determination of the structure of CF_3COOH faces two severe problems. First, both carbon atoms are near the the a-axis of the principal inertia tensor. This reduces the structural information contained in the rotational constants of the ^{13}C isotopomers. Second, no stable isotopomers exist for the fluorine atoms. This reduces the maximum number of monosubstituted isotopomers to five. Together with the three rotational constants of the parent species this corresponds to a total of 18 rotational constants.

To assist in the search for the low intensity spectra of the less abundant species and to complement the microwave spectroscopical investigation quantum chemical calculations based on the GAUSSIAN 94 program package [9] were carried out. At the final stage we used the MP2 method with the rather large 6-311++G** basis set provided with the program. These calculations turned out to be very helpful in the search for the rotational spectra of the less abundant isotopomers, and below we will demonstrate the usefullness of a method, which combines information from microwave spectroscopy and from such ab initio calculations to facilitate and speed up the assignment of low intensity isotopomer rotational spectra.

In the course of the present investigation we have also resolved and analysed the multiplet patterns of the rotational transitions of several low-J transitions of the CF_3COOD isotopomer. They are caused by the interaction of the deuterium nuclear quadrupole moment with the intramolecular electric field gradient at the position of the deuterium nucleus. With the nuclear quadrupole moment known, they provide information on the latter. These experimental quadrupole coupling constants too are compared to the results of ab initio calculations and in future investigations it will be interesting to see how their changes upon formation of hydrogen bridged complexes will correlate to the corresponding changes in the O-D bond distance. Finally we have calculated a MP2/6-311++G** minimum energy path for the CF_3 internal rotation for comparison with the internal rotation barrier determined in [7].

2. Experimental

Trifluoroacetic acid, 99 %, was purchased from Lancaster, Whitehand, England. It was used as received. The spectra of the ^{13}C isotopomers were recorded in natural abundance at Kiel with a MBMWFT spectrometer described in [10]. Since the rotational temperature rapidly drops to few degrees Kelvin within the first few mm downstream of the nozzle in the supersonic jet expansion, only the lowest rotational states are populated. This considerably facilitates the analysis as compared to the situation encountered by Stolwijck and van Eijck. At the same time, the monomer $\rightleftharpoons$ dimer equilibrium remains almost at its room temperature value, since the acid molecules predominantly collide with carrier gas atoms (He, Ne, or Ar) in the expansion region.

Subsequent to the analysis of the ^{13}C spectra the work was continued at Valladolid for the ^{18}O isotopomers. Their spectra too were recorded in natural abundance, using a more sensitive MBFTMW spectrometer. Its construction has been given in [11]. Finally, several hithertoo unknown low-J transitions of the deuterated isotopomer were measured at Kiel with a further improved MBMWFT spectrometer [12] in order to obtain information on the deuterium nuclear quadrupole coupling constants. For the new assignments the scan facilities [13] of the instruments were of great help.

For the ^{13}C isotopomers the sample was introduced with a content of 1 to 2 % using argon and, in fewer cases, neon as carrier gas with a backing pressure of about 0.5 bar. For the scans the transient decays of 2^{10} to 2^{11} experimental cycles were accumulated at each frequency setting prior to Fourier transformation. The frequency step width was 250 kHz. The final high resolution measurements for the isotopomer spectra were taken with 2^{13} to 2^{14} experimental cycles, 10 ns sampling interval and 2^{13} data points per free induction decay. For the ^{18}O isotopomers He was used as carrier gas at pressures near 1.5 bar. Typically 2^{13} data points were taken per free induction decay with 40 ns as sampling interval between two successive data points and 2^{11} transient emission signals were accumulated prior to the FT-analysis or decay-fit analysis [14, 15], respectively. The molecular pulse had a duration of 0.45 ms and the microwave polarisation pulse was applied after a delay of 0.3 ms with respect to the opening time of the nozzle.

For the recording of the deuterated species, the sample, a 1:2 mixture of D_2O and CF_3COOH, was provided in a heatable stainless steel container shortly upstream of the nozzle of the MBMWFT spectrometer with the carrier gas, helium, at an elevated backing

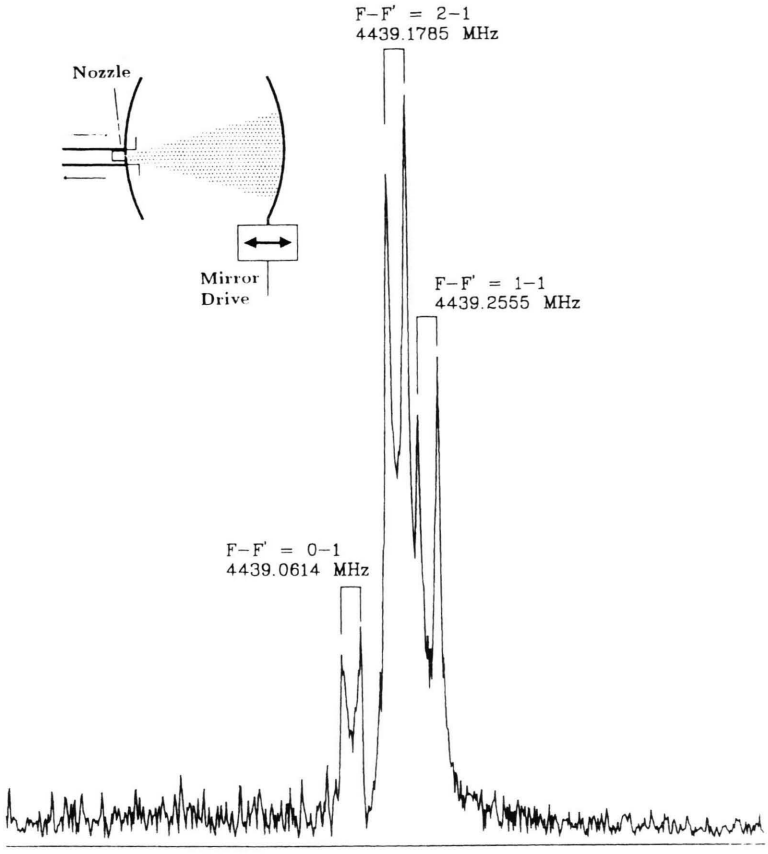

Fig. 1. CF_3COOD, deuterium nuclear quadrupole hyperfine triplet of the $1_{0\,1} - 0_{0\,0}$ rotational transition. A section of 1.88 MHz is presented. Each of the three hyperfine satellites is split into a doublet due to the Doppler-effect in the parallel beam configuration (see insert upper left). Helium was used as carrier gas. The observed Doppler-splitting of 45.4 kHz corresponds to a beam velocity close to 1.5 km/sec. Additional experimental informations: polarization frequency ν_{pol} = 4439.140 MHz; 16 k data points were taken for each free induction decay at a sampling interval of 10 ns; the final signal represents the sum of 2048 individual free induction decays.

pressure close to 1.3 bar. Typically 2^9 to 2^{11} transient emission signals were accumulated, each with 10 ns sampling interval and 2^{14} data points in the time domain. Helium was used rather than argon or neon in order to untangle the Doppler splitted deuterium nuclear quadrupole hyperfine multiplets. In Fig. 1 we present the Fourier transform amplitude spectrum of the $J'_{K'_-\,K'_+} - J''_{K''_-\,K''_+} = 1_{0\,1} - 0_{0\,0}$ rotational transition as an example. With 2^{14} data points taken at a sampling interval of 10 ns, the spectral point distance is 6.1035 kHz in this recording. For the final analysis, the satellite frequencies, amplitudes, phases, the decaytime and the Doppler splitting (beam velocity) were fitted to the observed transient emission signals by a Levenberg-Marquardt routine [16, 17].

In order to reduce the search ranges (scan ranges) for the initial assignment of the ^{13}C and ^{18}O spectra, the known rotational constants of the parent species and the results of a fully relaxed MP2/6-311++G** calculation were combined to predict the rotational constants of the isotopomers as follows:

$$A^{\text{exp,pred}}_{\text{daughter}} = A^{\text{exp}}_{\text{parent}} - A^{\text{MP2}}_{\text{parent}} + A^{\text{MP2}}_{\text{daughter}} \qquad (1)$$

(and cyclic permutations ($A \rightarrow B \rightarrow C$)). The success of this procedure depends on the degree of approximation to which our following two assumptions are fulfilled. First, we assume that the minimum energy MP2/6-311++G** structure closely reproduces the true equilibrium configuration. Second, we assume that the differences between the experimentally observed vibrational ground state expectation values for the rotational constants and the corresponding rigid rotor values, i.e. the vibrational contributions to the effective rotational constants, are very nearly the same for all isotopomers. If both assumptions were fulfilled exactly, (1) would lead to precise predictions. As it turned out, the predicted rotational constants indeed reproduced the experimental values within approximately 1 MHz and better. This reduced the searching range for the $J = 1 \rightarrow J = 0$ transitions of the less abundant species to about ± 2 MHz, which considerably speeded up their assignment.

Table 1. CF_3COOH, observed frequencies, rotational constants and quartic centrifugal distortion constants. Watson's A-reduction in the I^r-representation was used for the fit of the rotational constants and the centrifugal distortion constants to the observed frequencies.

J'	K'_-	K'_+	–	J''	K''_-	K''_+	exp. freq. MHz	exp. – calc. kHz
2	1	1	-	2	1	2	1270.7748	–1.4
1	1	0	-	1	0	1	1789.9310	0.4
2	1	1	-	2	0	2	2297.6770	–0.2
3	1	2	-	3	1	3	2530.8326	–1.5
3	1	2	-	3	0	3	3190.8530	0.5
4	2	2	-	4	1	3	3908.6210	–0.5
4	1	3	-	4	0	4	4530.4240	0.0
1	0	1	-	0	0	0	4573.9870	0.3
2	2	1	-	2	1	2	5369.7910	–0.5
1	1	1	-	0	0	0	5940.3270	–0.3
3	2	2	-	3	1	3	6053.4080	–0.2
4	2	3	-	4	1	4	6975.4060	–0.2
4	3	1	-	4	2	2	7123.5000	–0.8
3	3	0	-	3	2	1	7548.7170	–0.1
2	0	2	-	1	1	1	7697.4610	0.4
3	3	1	-	3	2	2	7938.9890	–0.2
5	3	3	-	5	2	4	8527.8117	2.4
2	1	2	-	1	1	1	8724.3659	–1.1
2	0	2	-	1	0	1	9063.8018	–0.9
6	3	4	-	6	2	5	9124.8611	1.7
2	1	1	-	1	1	0	9571.5466	–0.3
7	3	5	-	7	2	6	9958.9192	0.5
2	1	2	-	1	0	1	10090.7050	–0.8
7	1	6	-	7	0	7	10215.1366	–0.4
5	4	1	-	5	3	2	10646.1723	0.3
7	4	4	-	7	3	5	11116.6476	–0.3
8	4	5	-	8	3	6	11436.9669	–1.6
9	4	6	-	9	3	7	11969.3380	0.1
10	5	5	-	10	4	6	12009.3427	0.2
9	3	7	-	9	2	8	12310.9932	0.2
3	0	3	-	2	1	2	12378.2211	–0.5
3	1	3	-	2	1	2	13038.2417	1.3
8	5	3	-	8	4	4	13393.2544	0.0
3	0	3	-	2	0	2	13405.1222	1.8
2	2	1	-	1	1	0	13670.5640	–0.6
3	2	1	-	2	2	0	14038.6730	0.0
3	1	3	-	2	0	2	14065.1483	–1.9
2	2	0	-	1	1	1	14178.3224	0.5
3	1	2	-	2	1	1	14298.3003	0.4
4	0	4	-	3	1	3	16939.8291	–0.2
4	1	4	-	3	1	3	17307.5775	1.2
4	0	4	-	3	0	3	17599.8500	1.4
3	2	2	-	2	1	1	17820.8774	0.0
5	1	5	-	4	1	4	21535.1949	–0.6
5	0	5	-	4	0	4	21719.1349	–0.3
4	2	3	-	3	1	2	21752.1540	–0.6
5	2	4	-	4	2	3	22682.9992	0.8
5	3	3	-	4	3	2	23064.6353	–0.9
5	4	1	-	4	4	0	23064.8395	–0.3
5	3	2	-	4	3	1	23270.4386	0.4

Table I (continued).

$A^{(A)}$	/	MHz	3 865.132 93(11)
$B^{(A)}$	/	MHz	2 498.769 62(08)
$C^{(A)}$	/	MHz	2 075.218 71(07)
Δ_J	/	kHz	0.261 7(18)
Δ_{JK}	/	kHz	3.185 6(25)
Δ_K	/	kHz	–2.992 4(71)
δ_J	/	kHz	0.05108(27)
δ_K	/	kHz	–10.363 2(39)

Table 2. Predicted rotational constants (MHz) for the monosubstituted less abundant isotopomers. The predictions are based on the experimental rotational constants of the parent species, on the rotational constants calculated for the MP2/6-311++G** structure, and on the differences between the experimental and the MP2/6-311++G** rotational constants for the parent species (see Equation (1) of the text). Also given, for direct comparison, are the final experimental values for the rotational constants.

	$^{13}CF_3$-COOH	CF_3-^{13}COOH	CF_3-C^{18}OOH	CF_3-CO^{18}OH	CF_3-COOD
A_{MP2}	3838.973	3838.543	3767.189	3774.427	3812.836
A_{exp}^{pred}	3865.129	3864.699	3793.345	3800.577	3838.992
A_{exp}	3865.433	3864.807	3792.200	3800.967	3839.672
B_{MP2}	2495.624	2487.298	2437.472	2442.122	2424.318
B_{exp}^{pred}	2495.094	2486.759	2436.942	2441.592	2423.788
B_{exp}	2495.305	2486.955	2437.969	2440.812	2423.255
C_{MP2}	2066.610	2060.767	2006.391	2011.596	2010.230
C_{exp}^{pred}	2072.699	2066.855	2012.479	2017.684	2016.318
C_{exp}	2072.828	2066.972	2012.704	2017.132	2015.937

In Table 1 we present our rotational transition frequencies for the most abundant (parent) species. This Table extends the measurements reported in Table 3 of [7] to lower frequencies and J-quantum numbers and allows for an even more accurate fit of the rotational constants and centrifugal distortion constants for the parent species. In Table 2 we present our predictions for the rotational constants of the less abundant isotopomers. In Tables 3 through 6 the measured rotational spectra for the ^{13}C and ^{18}O isotopomers are given and in Table 7 we present satellite frequencies for several low-J D-hfs multiplets. They were measured for the determination of the deuterium quadrupole coupling constants and their inclusion in the centrifugal analysis of the CF_3COOD spectrum did lead to improved rotational constants for this isotopomer.

Table 3. $^{13}CF_3COOH$, observed frequencies, rotational constants and quartic centrifugal distortion constants. (Compare Table 1).

$J'\ K'_-\ K'_+ - J''\ K''_-\ K''_+$	exp. freq. MHz	exp. – calc. kHz
1 1 1 - 0 0 0	5938.2353	–1.0
2 0 2 - 1 0 1	9052.6770	0.2
2 1 2 - 1 1 1	8713.728	–0.4
2 1 1 - 1 1 0	9558.759	–0.9
2 1 2 - 1 0 1	10083.833	–0.1
2 0 2 - 1 1 1	7682.571	–1.1
2 2 0 - 1 1 1	14175.165	0.3
2 2 1 - 1 1 0	13669.067	–1.0
3 0 3 - 2 0 2	13389.612	1.4
3 1 3 - 2 1 2	13022.609	–0.5
3 1 2 - 2 1 1	14279.565	–1.5
3 2 2 - 2 2 1	13704.296	1.9
3 2 1 - 2 2 0	14019.054	2.2
3 1 3 - 2 0 2	14053.766	0.2
3 0 3 - 2 1 2	12358.454	–0.3
3 2 2 - 2 1 1	17814.603	0.8
4 0 4 - 3 0 3	17580.335	–1.5
4 1 4 - 3 1 3	17287.186	–0.2
4 2 3 - 3 2 2	18206.623	0.8
4 3 2 - 3 3 1	18412.463	–2.7
4 3 1 - 3 3 0	18474.257	1.0
4 1 4 - 3 0 3	17951.342	0.5
4 0 4 - 3 1 3	16916.182	0.7

$A^{(A)}$	/	MHz	3865.4333(10)
$B^{(A)}$	/	MHz	2495.3046(07)
$C^{(A)}$	/	MHz	2072.8281(07)
Δ_J	/	kHz	0.272(66)
Δ_{JK}	/	kHz	3.10 (28)
Δ_K	/	kHz	–2.48 (79)
δ_J	/	kHz	0.052(41)
δ_K	/	kHz	–10.23 (56)

Table 4. $CF_3^{13}COOH$, observed and calculated frequencies, rotational constants and quartic centrifugal distortion constants. (Compare Table 1).

$J'\ K'_-\ K'_+ - J''\ K''_-\ K''_+$	exp. freq. MHz	exp. – calc. kHz
1 1 1 0 0 0	5931.7535	0.8
2 0 2 1 1 1	7647.7381	–0.9
2 1 2 1 1 1	8687.8122	–0.6
2 0 2 1 0 1	9025.5648	0.7
2 1 1 1 1 0	9527.8529	1.5
2 1 2 1 0 1	10065.6418	–1.9
3 0 3 2 1 2	12311.4805	–1.1
3 1 3 2 1 2	12984.4466	0.8
3 0 3 2 0 2	13351.5543	–0.5
2 2 1 1 1 0	13661.3333	0.6
3 2 2 2 2 1	13661.6748	2.1
3 2 1 2 2 0	13971.8739	0.1
3 1 3 2 0 2	14024.5232	–1.4
2 2 0 1 1 1	14163.6396	–2.8
3 1 2 2 1 1	14234.1883	1.1
4 0 4 3 1 3	16859.2832	–0.6
4 1 4 3 1 3	17237.3132	0.7
4 0 4 3 0 3	17532.2495	1.1
3 2 2 2 1 1	17795.1542	2.2
4 1 4 3 0 3	17910.2822	–0.2
4 2 3 3 2 2	18150.8352	–1.1
4 3 2 3 3 1	18353.6850	–2.3
4 3 1 3 3 0	18413.9259	1.3

$A^{(A)}$	/	MHz	3864.8071(12)
$B^{(A)}$	/	MHz	2486.9553(9)
$C^{(A)}$	/	MHz	2066.9719(6)
Δ_J	/	kHz	0.285(22)
Δ_{JK}	/	kHz	3.079(93)
Δ_K	/	kHz	–2.49 (26)
δ_J	/	kHz	0.073(14)
δ_K	/	kHz	–10.09 (19)

3. Analysis and Results

3.1. Rotational Constants, Centrifugal Distortion Constants and D-hfs Coupling Constants

The spectra of the ^{13}C -, ^{18}O, and the parent species were analysed with the model of a centrifugally distorted rotor [18] using Watsons A-reduction in the I^r-representation [19]:

$$\hat{H}_{\text{eff}}^{(A)} = A^{(A)}\hat{J}_a^2 + B^{(A)}\hat{J}_b^2 + C^{(A)}\hat{J}_c^2 - \Delta_J\hat{J}^4 \qquad (2)$$
$$- \Delta_{JK}\hat{J}^2\hat{J}_a^2 - \Delta_K\hat{J}_a^4 - 2\delta_J\hat{J}^2\left(\hat{J}_b^2 - \hat{J}_c^2\right)$$
$$- \delta_K\left[\hat{J}_a^2\left(\hat{J}_b^2 - \hat{J}_c^2\right) + \left(\hat{J}_b^2 - \hat{J}_c^2\right)\hat{J}_a^2\right].$$

Here $\hat{J}_g$, $(g = a, b, c)$ are the angular momentum operators in units of $\hbar$ with respect to the molecular center of mass system, $G^{(A)}, (G = A, B, C)$ are effective rotational constants and Δ_J, Δ_{JK} etc. are the quartic centrifugal distortion constants (compare too (8.97) through (8.99) in [20], where the misprinted sign of Δ_J has been corrected). The program ZFAP4, written by Typke, now at the University of Ulm [21], was used. The deuterium nuclear quadrupole hyperfine multiplets given in Table 7 were analysed with the program XIAM, written by Hartwig [22]. In this program the matrix of the effective rotational Hamiltonian, including D-hfs interaction, centrifugal distortion, and, optionally, internal rotation, is diagonalized numerically. In the present application internal rotation could be neglected. Due to the large value of the moment of inertia of the CF_3-top around its internal

Table 5. $CF_3C^{18}OOH$, observed frequencies (MHz), rotational constants and quartic centrifugal distortion constants (Compare Table 1).

$J'\ K'_-\ K'_+ - J''\ K''_-\ K''_+$	exp. freq. MHz	exp. – calc. kHz
1 1 1 - 0 0 0	5804.879	–1.3
2 0 2 - 1 0 1	8815.902	–1.3
2 1 2 - 1 1 1	8476.021	–0.9
2 1 1 - 1 1 0	9326.627	–0.8
2 1 2 - 1 0 1	9830.233	2.7
2 2 1 - 1 1 0	13389.251	0.5
3 0 3 - 2 0 2	13030.808	–0.8
3 1 3 - 2 1 2	12665.043	0.3
3 1 2 - 2 1 1	13929.951	0.6
3 2 2 - 2 2 1	13351.915	–0.8
3 2 1 - 2 2 0	13673.096	0.6
3 1 3 - 2 0 2	13679.371	1.3
3 2 2 - 2 1 1	17414.538	–0.5
4 0 4 - 3 0 3	17098.508	–0.1
4 1 4 - 3 1 3	16809.037	2.9
4 1 3 - 3 1 2	18446.097	–0.9
4 2 3 - 3 2 2	17735.312	0.9
4 1 4 - 3 0 3	17457.592	–3.0
4 0 4 - 3 1 3	16449.947	–0.2

$A^{(A)}$	/	MHz	3792.2004(18)
$B^{(A)}$	/	MHz	2437.9694(11)
$C^{(A)}$	/	MHz	2012.7036(08)
Δ_J	/	kHz	0.283(24)
Δ_{JK}	/	kHz	3.03 (9)
Δ_K	/	kHz	–2.71 (35)
δ_J	/	kHz	0.059(12)
δ_K	/	kHz	–9.74 (27)

Table 6. $CF_3CO^{18}OH$, observed frequencies (MHz), rotational constants and quartic centrifugal distortion constants (Compare Table 1).

$J'\ K'_-\ K'_+ - J''\ K''_-\ K''_+$	exp. freq. MHz	exp. – calc. kHz
1 1 1 - 0 0 0	5818.073	.000
2 0 2 - 1 0 1	8831.343	.002
2 1 2 - 1 1 1	8492.148	.000
2 1 1 - 1 1 0	9339.587	.000
2 1 2 - 1 0 1	9852.282	.003
2 2 1 - 1 1 0	13419.976	–.001
3 0 3 - 2 0 2	13055.742	–.002
3 1 3 - 2 1 2	12689.720	–.001
3 1 2 - 2 1 1	13950.069	–.002
3 2 2 - 2 2 1	13373.729	–.001
3 2 1 - 2 2 0	13691.791	.000
3 1 3 - 2 0 2	13710.658	–.001
3 2 2 - 2 1 1	17454.122	.001
4 0 4 - 3 0 3	17133.496	–.002
4 1 4 - 3 1 3	16842.627	.001
4 1 3 - 3 1 2	18474.452	.000
4 2 3 - 3 2 2	17765.110	.000
4 2 2 - 3 2 1	18462.183	.000
4 0 4 - 3 1 3	16478.585	.002

$A^{(A)}$	/	MHz	3800.9666(18)
$B^{(A)}$	/	MHz	2440.8119(08)
$C^{(A)}$	/	MHz	2017.1317(07)
Δ_J	/	kHz	0.243(14)
Δ_{JK}	/	kHz	3.10 (07)
Δ_K	/	kHz	–2.80 (35)
δ_J	/	kHz	0.057(10)
δ_K	/	kHz	–10.21 (17)

rotation axis, tunneling is negligible and the internal rotation splittings in the ground torsional state are far below the resolution power of the spectrometer even though the barrier to internal rotation of the CF_3 top is well below 1 kcal/mole (V_3^{exp} = 0.691(2) kcal/mole, see [7]).

The rotational constants, centrifugal distortion constants, and – in the case of the deuterated species – the nuclear quadrupole coupling constants, which enter into the effective Hamiltonian and which were fitted to the observed transition frequencies are given at the bottom of the frequency Tables 1, and 3 through 7.

In Table 8 we present the "determinable rotational constants" for all mono substituted isotopomers [23].

$$\begin{aligned} A &= A^{(A)} + 2 \cdot \Delta_J \\ B &= B^{(A)} + 2 \cdot \Delta_J + \Delta_{JK} - 2 \cdot \delta_J - \delta_K \\ C &= C^{(A)} + 2 \cdot \Delta_J + \Delta_{JK} + 2 \cdot \delta_J + \delta_K \end{aligned} \qquad (3)$$

They differ slightly from the effective rotational constants for the A-reduced Hamiltonian in so far, as the centrifugal contributions to their values have been eliminated as far as possible. They represent the best approximations to the vibrational ground state expectation values of the rotational constants, which can be derived from our experimental information and were used for the determination of the structure (see below). Also presented for comparison are the corresponding values for the energy relaxed MP2/6-311++G** structure and the differences between the rotational constants of the substituted compounds (daughter molecules) and the rotational constants of the most abundant species (parent compound). As is obvious from Table 8, corresponding experimental and ab initio differences are indeed very close to each other. As pointed out already, this may indicate that the MP2/6-311++G** calculation does lead to a structure rather close to the equilibrium configuration, a result which has been pointed out already earlier by Marstokk and Møllendal [24]. It also indicates that for trifluoroacetic acid the vibra-

Table 7. Deuterium quadrupole hyperfine multiplets of low-J rotational transitions. The calculated hfs-splittings, $\Delta\nu_{hfs,calc}$ are given with respect to the hypothetical center frequency of the multiplet ($\Delta\nu_{hfs,exp} - \Delta\nu_{hfs,calc}$-values are given in brackets in units of the least significant figure). The experimental center frequency (first column) represents an average, calculated from the observed satellite frequencies and the corresponding $\Delta\nu_{hfs,calc}$ values. At the bottom of the Table the deuterium quadrupole coupling constants, rotational constants and quartic centrifugal distortion constants of CF_3COOD are listed.

$J'K'_-K'_+ - J''K''_-K''_+$ ν_{center}/MHz	F'-F''		ν_{obs} MHz	$\Delta\nu_{hfs,calc}$ kHz	Rel. int. %
101-000	2	1	4439.1785	−12.9 (5)	55.56
4439.1909	1	1	4439.2555	64.4 (2)	33.33
	0	1	4439.0614	−128.7 (−8)	11.11
111-000	2	1	5855.5904	5.9 (−3)	55.56
5855.5848	1	1	5855.5557	−29.5 (4)	33.33
	0	1	5855.6438	59.0 (0)	11.11
202-101	3	2	8802.4249	−5.3(−15)	46.67
8802.4317	2	1	–	−0.8	25.00
	1	0	8802.4984	65.2 (15)	11.11
	1	1	8802.3039	−127.9 (1)	8.33
211-110	3	2	9285.7084	−15.4 (2)	46.67
9285.7218	2	1	9285.7869	64.4 (7)	25.00
	1	0	9285.6200	−99.2(−26)	11.11
212-111	3	2	8470.9898	−15.9(−14)	46.67
8471.0071	2	1	8471.0734	64.4 (19)	25.00
	1	0	8470.9127	−93.8 (−6)	11.11
221-212	3	3	5471.2822	28.4 (−5)	41.48
5471.2543	2	2	5471.1555	−99.2 (−4)	23.15
212-101	3	2	9887.4046	2.9 (3)	46.67
9887.4014	2	1	9887.3717	−29.5 (−2)	25.00
	1	0	9887.4954	93.8 (2)	11.11
	2	2	9887.4487	47.7 (−4)	8.33
202-111	3	2	7386.0110	−24.1 (−1)	46.67
7386.0352	2	1	7386.1280	93.0 (−2)	25.00
	1	0	7385.9130	−122.5 (3)	11.11
330-321	4	4	7789.4607	27.3(−18)	40.18
7789.4352	3	3	7789.3552	−81.8 (18)	28.01
	2	2	7789.5008	65.5 (1)	21.16

$A^{(A)}$	/	MHz	3839.6716(8)
$B^{(A)}$	/	MHz	2423.2554(8)
$C^{(A)}$	/	MHz	2015.9370(8)
Δ_J	/	kHz	0.26 (10)
Δ_{JK}	/	kHz	2.91 (41)
Δ_K	/	kHz	−2.81 (39)
Δ_J	/	kHz	0.045(93)
Δ_K	/	kHz	−10.2 (13)
$\chi_{bb} + \chi_{cc}$	/	kHz	−257.4 (5)
$\chi_{bb} - \chi_{cc}$	/	kHz	21.6(18)

tional corrections are rather similar for all isotopomers.

Table 8. Centrifugal corrections, $\Delta A_{cd} = 2 \cdot \Delta_J$, $\Delta B_{cd} = 2 \cdot \Delta_J + \Delta_{JK} - 2\delta_J - \delta_K$, $\Delta C_{cd} = 2\Delta_J + \Delta_{JK} + 2\delta_J + \delta_K$ and determinable vibronic ground state rotational constants, A, B, C, for the parent species and all monosubstituted isotopomers. Also given are the differences between the experimental rotational constants of the daughter molecules with respect to the parent molecule as well as their quantum chemical counterparts, calculated from the MP2/6-311++G** minimum energy structure.

	CF_3COOH	$^{13}CF_3COOH$	$CF_3^{13}COOH$
$A^{(A)}$/MHz	3865.1330	3865.4333	3864.8063
ΔA_{cd}/kHz	0.53	0.54	0.58
A/MHz	3865.1335	3865.4338	3864.8069
$(A^{MP2} - A^{MP2}_{parent})$/MHz		−0.004	−0.434
$(A^{exp} - A^{exp}_{parent})$/MHz		+0.300	−0.327
$B^{(A)}$/MHz	2498.7697	2495.3046	2486.9549
ΔB_{cd}/kHz	24.32	24.00	23.47
B/MHz	2498.7940	2495.3286	2486.9784
$(B^{MP2} - B^{MP2}_{parent})$/MHz		−3.676	−12.011
$(B^{exp} - B^{exp}_{parent})$/MHz		−3.465	−11.816
$C^{(A)}$/MHz	2075.2188	2072.8280	2066.9722
ΔC_{cd}/kHz	−16.90	−16.71	−16.24
C/MHz	2075.2019	2072.8113	2066.9560
$(C^{MP2} - C^{MP2}_{parent})$/MHz		−2.521	−8.364
$(C^{exp} - C^{exp}_{parent})$/MHz		−2.391	−8.246

	$CF_3C^{18}OOH$	$CF_3CO^{18}OH$	CF_3COOD
$A^{(A)}$/MHz	3792.1999	3800.9669	3839.6717
ΔA_{cd}/kHz	0.55	0.48	0.53
A/MHz	3792.2005	3800.9674	3839.6722
$(A^{MP2} - A^{MP2}_{parent})$/MHz	−71.788	−64.556	−26.141
$(A^{exp} - A^{exp}_{parent})$/MHz	−72.934	−64.167	−25.462
$B^{(A)}$/MHz	2437.9689	2440.8120	2423.2557
ΔB_{cd}/kHz	23.17	23.89	23.75
B/MHz	2437.9921	2440.8359	2423.2794
$(B^{MP2} - B^{MP2}_{parent})$/MHz	−61.828	−57.178	−74.982
$(B^{exp} - B^{exp}_{parent})$/MHz	−60.802	−57.958	−75.515
$C^{(A)}$/MHz	2012.7040	2017.1315	2015.9369
ΔC_{cd}/kHz	−15.97	−16.71	−16.87
C/MHz	2012.6880	2017.1148	2015.9201
$(C^{MP2} - C^{MP2}_{parent})$/MHz	−62.740	−57.535	−58.901
$(C^{exp} - C^{exp}_{parent})$/MHz	−62.514	−58.087	−59.282

3.2. Determination of the Structure

In Fig. 2 we display the structure of CF_3COOH for easy referencing. Assuming a symmetry plane for the equilibrium structure, such as is suggested from the MP2/6-311++G** results, twelve structural parameters have to be determined. From the experimental point of view, the 18 experimental rotational constants and the corresponding moments of inertia form

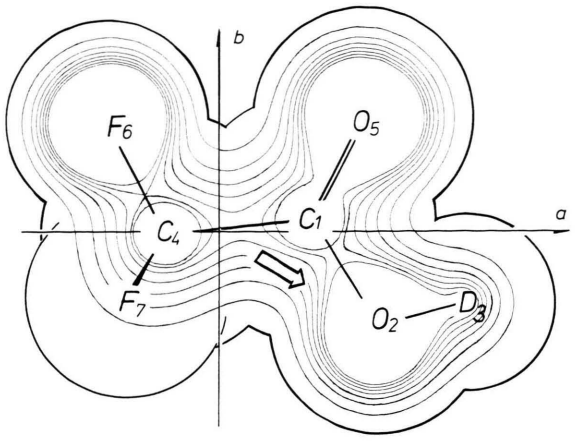

Fig. 2. Minimum energy configuration of trifluoroacetic acid with numbering of the atoms. Also shown are the principal inertia axes and the orientation of the electric dipole moment from the MP2/6-311++G** calculation (μ_a = 1.91 D, μ_b = −1.19 D).

the basis of their determination. The practically identical values of the rigid-rotor planar moments,

$$\frac{h}{16 \cdot \pi^2} \cdot \left(\frac{1}{A} + \frac{1}{B} - \frac{1}{C}\right) = \sum_{n=1}^{n=8} m_n \cdot c_n^2 \qquad (4)$$

$$= 44.73 \pm 0.01 \text{ amu Å}^2,$$

for all isotopomers indicate, in agreement with the MP2-result, that all substituted atoms lie in a plane of symmetry of the moment of inertia tensor which coincides with a planar frame of the molecule.

To derive structural parameters from the observed rotational constants we have used two different methods. Both methods rely on the assumption that the vibrational contributions to the observed rotational constants are largely the same for all isotopomers and will thus cancel to a high degree of approximation, if only differences of corresponding rotational constants or moments of inertia are used to derive the structural parameters. In both methods the observed moments of inertia and rotational constants are therefore treated as if the molecules were rigid with all atoms locked to their equilibrium positions.

In the first method, termed r_s-method [6], which was introduced by Kraitchman [25] and Costain [26], the coordinates of the substituted atom with respect to the principal inertia axes system of the most abundant species are calculated from the differences in the inverse rotational constants of the isotopomer with respect to the corresponding inverse rotational constants of the most abundant species. Rudolph's program RU233 [27] was used in this context. The resulting atom coordinates with respect to the principal inertia axes system of the most abundant species are presented in Table 9. The uncertainties in the r_s-coordinates were estimated according to van Eijck [28]. We note that the r_s-method leads to an imaginary value for the b-coordinate of $C_{(4)}$. This demonstrates the limitations of the r_s-method in cases where atoms are located close to a principal inertia axis. In the present case for instance, with $C_{(4)}$ close to the a-axis, the moments of inertia depend very little on the small b- and c-coordinate of this atom in all isotopomers and the model error caused by incomplete compensa-

Table 9. Cartesian principal inertia axes system coordinates (Å) of the atoms in CF_3COOH as determined from the differences in the moments of inertia (r_s-coordinates), from the differences in the rotational constants of the five isotopomers with respect to the corresponding rotational constants of the parent species (ΔG-coordinates) and from the fully relaxed MP2/6-311++G** ab initio structure (MP2-coordinates). For the atom indices compare Figure 2. For the r_s-coordinates the asterix indicates an imaginary value. Six decimal figures are given only for the numerical comparison with the experimental values of the rotational constants. For r_s the uncertainties are estimated according to van Eijck [28].

Index	Atom	Method	a_n	b_n	c_n
1	C	r_s	0.9827(8)	0.1054(70)	0.012(68)
		ΔG	0.985049	0.106847	0.000000
		MP2	0.990738	0.123115	0.000000
2	O	r_s	1.5374(4)	−1.0940(7)	0.027892*
		ΔG	1.539866	−1.100683	0.000000
		MP2	1.525444	−1.104467	0.000000
3	H	r_s	2.4980(12)	−0.9708(30)	0.070(45)
		ΔG	2.503177	−0.978899	0.000000
		MP2	2.487920	−0.992477	0.000000
4	C	r_s	−0.5362(15)	0.071583*	0.000000
		ΔG	−0.532666	0.007092	0.000000
		MP2	−0.547234	0.011312	0.000000
5	O	r_s	1.5723(4)	1.1698(5)	0.036788*
		ΔG	1.574584	1.176734	0.000000
		MP2	1.584781	1.168857	0.000000
6	F	r_s	–	–	–
		ΔG	−1.095333	1.213278	0.000000
		MP2	−1.101474	1.217323	0.000000
7	F	r_s	–	–	–
		ΔG	−0.972638	−0.648672	1.087903
		MP2	−0.964580	−0.651897	1.085869
8	F	r_s	–	–	–
		ΔG	−0.972638	−0.648672	−1.087903
		MP2	−0.964580	−0.651897	−1.085869

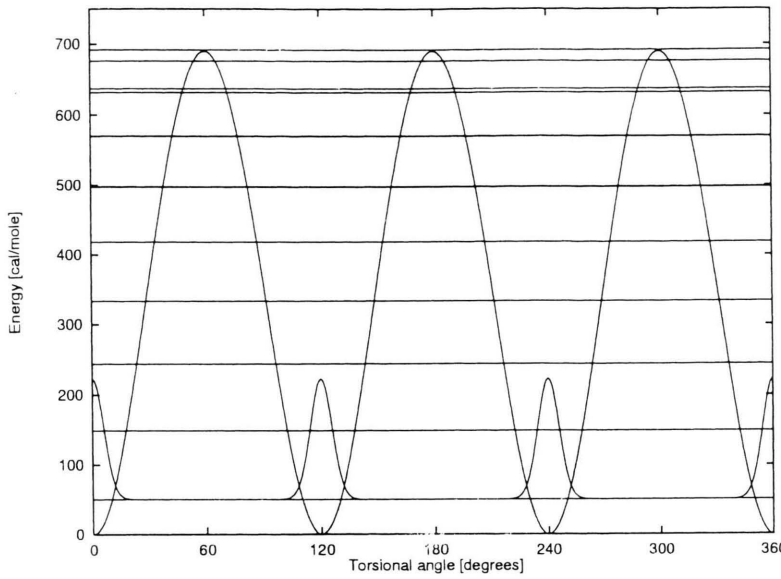

Fig. 3. Potential function for the CF_3-top internal rotation.

$$V(\tau) = \frac{V_3}{2}(1 - \cos(3\tau)) + \frac{V_6}{2}(1 - \cos(6\tau)).$$

Also shown are the lowest torsional energy levels, and the torsional ground state probability density. For comparison: the MP2/6-311++G** minimum energy path values for V_3 and V_6 are 629.3 cal/mole and 18.1 cal/mole, respectively (see text).

Table 10. Structural parameters of trifluoroacetic acid (distances in Å and bond angles and dihedral angle in degrees).

Parameter	substitution structure	least-squares fit to ΔG's	*ab initio* MP2/ 6-311++G**	*ab initio* hf/ 6-311++G**
$r(C_1O_2)$	1.3215	1.3294	1.3390	1.3115
$r(H_3O_2)$	0.9684	0.9713	0.9690	0.9472
$r(C_4C_1)$	1.5225	1.5210	1.5420	1.5378
$r(O_5C_1)$	1.2167	1.2219	1.2027	1.1716
$r(F_6C_4)$	–	1.3309	1.3273	1.3019
$r(F_7C_4)$	–	1.3445	1.3391	1.3123
$r(F_8C_4)$	–	1.3445	1.3391	1.3123
$\angle(H_3O_2C_1)$	107.51	107.52	106.90	109.92
$\angle(C_4C_1O_2)$	110.81	110.90	109.38	110.32
$\angle(C_4C_1O_5)$	122.95	122.60	123.76	123.13
$\angle(F_6C_4C_1)$	–	111.24	110.52	110.63
$\angle(F_7C_4C_1)$	–	111.01	110.28	110.15
δ (2-1-4-7)	–	±60.10	± 59.83	±59.78

tion of vibrational contributions gains in importance. Also given in Table 9 are the atom coordinates resulting from the least squares fit to the differences in the rotational constants (see below) and the MP2/6-311++G** minimum energy coordinates calculated with the GAUSSIAN 94 program package.

In the second method, introduced by Nösberger et al. [29], the differences of the rotational constants of the daughter molecules with respect to the corresponding rotational constants of the parent molecule, chosen as the most abundant species, are used directly and the structural parameters are adjusted for an optimal fit to these differences in a least squares procedure. Typkes program MWSTR1 [30] was used in this context. For the fit we have assumed C_s symmetry of the molecular frame and we have chosen the MP2/6-311++G** minimum energy structure as starting point. It turned out that, due to correlation, at most 11 parameters could be fitted simultaneously. Therefore the angles $< CCF_{in-plane}$ and $< CCF_{out-of-plane}$ were varied synchroneously, starting from their initial values as provided by the ab initio calculation. The highest correlation coefficient in this 11-parameter fit was 0.93. The resulting bond lengths and bond angles are presented in Table 10. Also presented in Table 10 are those structural parameters, which can be calculated from the r_s coordinates of the substituted atoms, ^{13}C, ^{18}O, and D. The parameters involving $C_{(4)}$ were calculated with the assumption $b_{C(4)} = 0.01$ Å taken from the MP2-calculation. We note that since the C-C-bond closely parallels the molecular a-axis, a change of ± 0.01 Å has only little effect on the bond length $r_{(CC)}$ and the bond angles $\angle CCO$.

3.3. Quantum Chemical Results for the Barrier to Internal Rotation and for the D-coupling Constants

3.3.1. Internal F_3C-top rotation

For comparison with the experimental result of Stolwijk and van Eijck we have also used the Gaussian 94 program package to run a minimum energy path

calculation for the internal rotation of the CF_3 top with respect to the carboxylic frame. Because of computer time limitations, the planarity condition was imposed on the CCOOH-frame and the otherwise fully energy relaxed configurations were calculated for three values of the internal rotation angle α, i.e. for three values of the dihedral angle 6-4-1-2 (compare Figure 2). Again the MP2 method was used with the standard 6-311++G** basis set. In Fig. 3 we present the torsional potential function, the lowest torsional energy levels with respect to the principal inertia axes reference system [31], and the probability density distribution function in the torsional ground state. From the MP2/6-311++G** calculation the in-plane C-F bond is cis to the C=O double bond at the bottom of the barrier, while the configuration with the in-plane C-F bond cis to the OH group corresponds to the top of the barrier. (Since no stable fluorine isotopes exist, it was not possible to determine the equilibrium orientation of the CF_3 top from microwave spectroscopy alone). With a calculated values of V_3^{MP2} = 629 cal/mole and V_6^{MP2} = 18 cal/mole, the ab initio barrier is about 9% lower than the experimental value V_3^{exp} = 691 cal/mole reported in [7]. Since the wave packet motion, corresponding to internal rotation will not exactly follow the minimum energy path, it appears reasonable that the experimental value for the barrier height should be higher than the minimum energy path value. Further, if one keeps in mind that the difference between the ab initio value and the experimental value not only reflects basis set and method errors in the ab initio values but also possible deficiencies in the rigid top rigid frame model, which has been used for the evaluation of the observed torsional splittings in the v = 4 torsional mode [7], the experimental and the ab initio values for the torsional barrier appear to be in fair agreement.

3.3.2. Comparison of the observed deuterium quadrupole coupling constants with Huber's empirical formula and with ab initio results

a) General remarks

The spectroscopic quadrupole coupling constants of the n-th nucleus relate to the anisotropies in the intramolecular electric field gradient tensor at the n^{th} nucleus under consideration as

$$\chi_{xx}(n) = \frac{e^2 \cdot Q_n}{a_0^3 \cdot h} \Big\langle 0 \Big| \Big(V_{xx}(\vec{r}_n) - \frac{V_{xx}(\vec{r}_n) + V_{yy}(\vec{r}_n) + V_{zz}(\vec{r}_n)}{3} \Big) \Big| 0 \Big\rangle, \tag{5}$$

$$\chi_{xy}(n) = \frac{e^2 \cdot Q_n}{a_0^3 \cdot h} \cdot \langle 0 | V_{xy}(\vec{r}_n) | 0 \rangle \tag{6}$$

(and cyclic permutations). Here $V_{xx}(\vec{r}_n)$, $V_{xy}(\vec{r}_n)$ etc. designate the second derivatives of the intramolecular Coulomb potential (in atomic units) at the position of nucleus, $\vec{r}_n$, as caused by the charge distribution of the other nuclei and the electrons. e, Q_n, a_0, h are the electronic charge, the nuclear quadrupole moment ($Q_n = 2.86 \cdot 10^{-27}$ cm^2 for the deuterium nucleus [32]), Bohr's radius, and Planck's constant, respectively. The brackets, $\langle 0| \ldots |0\rangle$ indicate vibronic ground state expectation values.

b) Huber's formula

Gerber and Huber [33] have proposed a surprisingly accurate formula for quick "back of the envelope" predictions of deuterium coupling constants, which relates

$$q_{\mathrm{bond}} = V_{\xi\xi} - \frac{V_{\xi\xi} + V_{\eta\eta} + V_{\zeta\zeta}}{3} \tag{7}$$

(ξ-axis in direction of the bond) to the bond distance, r, and to the electronegativities of the neighbouring atoms. Written in atomic units it reads

$$q_{\mathrm{bond}} = \Big[(Z_v - a) \Big(1 - \frac{1}{1 + b\,(\langle r \rangle / r)^5} \Big) + c\Delta \Big] \frac{2}{r^3}. \tag{8}$$

Z_{v} is the number of valence electrons and $\langle r \rangle$ is the average orbital radius on the neighbouring atom as discussed in [34]. $a = 1.875, b = 72.6, c = -0.029$ are parameters derived by Huber et al. from a fit to MP4SDQ-values for 35 molecules. r is the actual bond distance measured in Bohr's radii, and Δ is the (sum of the) difference(s) of Pauling's electronegativities between the second neighbour(s) and the neighbour atom (Δ = 1, compare App. G in [6] in the present application). Within the frame of (8) we assumed sp^3 hybridisation for the neighbour oxygen atom. This leads to $\langle r \rangle = (1 \cdot 0.6 + 3 \cdot 0.67)/4$ for the average orbital radius (see Table IV in [34]). Depending on the bond distance, $r_{(\mathrm{OD})}$, (8) predicts

the following values fo the coupling constant in bond direction

$$r_{(OD)} = 0.96\ \text{Å} \rightarrow \chi_{bond} = 255.46\ \text{kHz},$$
$$r_{(OD)} = 0.97\ \text{Å} \rightarrow \chi_{bond} = 237.87\ \text{kHz},$$
$$r_{(OD)} = 0.98\ \text{Å} \rightarrow \chi_{bond} = 221.49\ \text{kHz}.$$

This indicates that an uncertainty of 0.01 Å in the bond distance will correspond to an uncertainty of approximately 17 kHz in the calculated coupling constant.

c) Ab initio calculations of the field gradient anisotropies and coupling constants

Within the GAUSSIAN program package it is possible to calculate the electronic ground state expectation values for the second derivatives, $V_{xx}(\vec{r}_n), V_{xy}(\vec{r}_n)$ etc., at the right hand sides of (5) and (6). We note that for comparison with the experimental values the GAUSSIAN results must be transformed from the so called "standard system" (the x, y, z-system), which is used in the *ab initio* program, to the principal inertia axes system (the a, b, c-system) of the molecular mass distribution:

$$V_{aa} = \cos^2(\phi_{ax})V_{xx} + 2\cos(\phi_{ax})\cos(\phi_{ay})V_{xy} + \cos^2(\phi_{ay})V_{yy}, \tag{9}$$

$$V_{ab} = \cos(\phi_{ax})\cos(\phi_{bx}) \cdot V_{xx} + \left(\cos(\phi_{ax})\cos(\phi_{by}) + \cos(\phi_{ay})\cos(\phi_{bx})\right) V_{xy} + \cos(\phi_{ay})\cos(\phi_{by})V_{yy} \tag{10}$$

(and cyclic permutations). The angles, ϕ_{ax} etc., between the two coordinate systems were calculated from the MP2/6-311++G** equilibrium configuration (see Table 10).

The quality of the *ab initio* values clearly depends on the size and quality of the basis set and on the method used for the computation. We therefore tried several basis sets and two methods. Our final *ab initio* results for the field gradient anisotropies at the in-plane nuclei of CF_3COOD are presented in Figure 4. Note that the orders of magnitude of the field gradient anisotropies at the deuterium nucleus and at the carbon nuclei are about the same. From the simplified Townes-Dailey model [35], one would have expected a different result. Within this model the field gradient is attributed to the unequal filling of the p-orbitals of the valence shell of the atom under consideration.

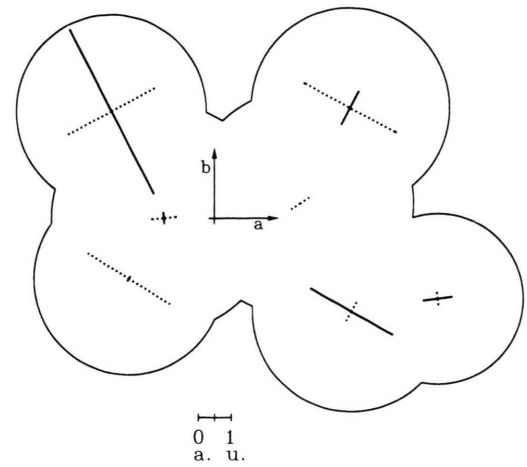

Fig. 4. Pictorial presentation of the ab initio electric field gradient asymmetry tensors at the in-plane nuclei of CF_3COOD. The lengths of the principal axes shown are proportional to the corresponding q-values (Compare the insert for the scale in atomic units). The axes, which point into the direction of a negative value for the anisotropy in the second derivatives of $V_{Coulomb}$, are drawn as boldface lines.

Therefore one would have expected the field gradients at the carbon nuclei (where p-orbitals are available) to be considerably larger than those at the deuterium nucleus (where only the spherical s-orbital but no p-orbitals are available to the first approximation).

The ab initio results for the deuterium quadrupole coupling constants are presented in Table 11. In this Table the prefixes HF and MP2 indicate the method (Hartree-Fock SCF and second order Møller-Plesset perturbation theory [36], respectively). The standard GAUSSIAN basis sets 6-311G, 6-311G** (including polarisation functions), and 6-311++G** (including additional diffuse valence shell GTO's) were used. In addition we tried Huzinagas [37] 6s+4p+4d basis (uncontracted) at the deuterium nucleus and the TZVP and TZV2P basis functions developed by Schäfer, Horn, and Ahlrichs [38] at the second row atoms C,F (TZVP) and O (TZV2P), respectively. For the convenience of the reader the latter bases are given in the Appendix. All calculations were performed at the MP2/6-311++G** structure.

The idea to use basis sets with high local quality (here Huzinaga's basis at the hydrogen (deuterium) nucleus, as a compromise between computer time and accuracy has been introduced with considerable success by Huber [33, 34, 39]. Obviously the higher flexibility of the basis set in the close vicinity of the

Table 11. Experimental and *ab initio* results for the D-hfs coupling constants in CF_3COOD. The *ab initio* values have been derived from the GAUSSIAN 94 electric field gradients calculated at the energy relaxed MP2/6-311++G** structure. For the designation of the ab initio methods and basis sets compare the text. In the last column, the corresponding calculated *ab initio* quadrupole coupling constant for the hydrogen molecule, HD, is presented for comparison. The approximate local mode vibrational correction to the coupling constants applied here appearently underestimates the true value roughly by a factor of two (see text).

Method/basis set	χ_{aa} /kHz	χ_{bb} /kHz	χ_{cc} /kHz	χ_{ab} /kHz	$\chi_{\|\|(HD)}$ /kHz
HF/6-311G	311.9	−134.9	−177.0	41.0	256.7
MP2/6-311G	321.1	−141.8	−179.3	45.0	254.4
HF/6-311G**	287.2	−122.4	−164.7	51.7	248.2
MP2/6-311G**	297.3	−129.8	−167.6	54.3	246.9
HF/6-311++G**	286.5	−121.9	−164.7	50.9	248.2
MP2/6-311++G**	296.6	−129.2	−167.5	53.1	246.9
HF/HUZ; 6-311G*	268.1	−113.4	−154.7	47.7	
MP2/HUZ; 6-311G*	281.2	−122.2	−159.0	50.2	
HF/HUZ; SHA	266.5	−111.9	−154.6	48.6	235.4
MP2/HUZ; SHA	279.1	−120.7	−158.4	50.8	233.3
vib. correction	−10.2	+2.3	+7.9		
MP2/HUZ; SHA + vib. corr.	268.9	−118.4	−150.5		
exp. values	257.4(5)	−117.9(10)	−139.5(10)		

nucleus under consideration far outweighs the errors which are introduced by the artificial shift of electron density into the region where the larger basis set is centered. This is the consequence of the fact that only the anisotropies in the electric field gradients are of interest for the quadrupole coupling constants. In Table 11, the pronounced effect of the locally increased flexibility is demonstrated in rows seven and eight, where Huzinaga's considerably more flexible basis was used at deuterium in combination with the standard 6 − 311G* basis, provided with the GAUSSIAN 94 program, at all second row atoms.

The much smaller effect of adding flexibility beyond that of the 6 − 311++G^* basis at the other nuclei is demonstrated at the bottom of Table 11. Here the coupling constants were calculated using Huzinagas 6s+4p+4d basis at D and the 6-311++G** basis at the heavy nuclei was replaced by the bases developed by Schäfer, Horn, and Ahlrichs [38] at O (TZV2P), C (TZVP), and F (TZVP) (compare the Appendix). As expected, the resulting higher flexibility at the second row nuclei leads to lower energies and a more even distribution of the electron density, as judged by the Mulliken atom charges, but it improves the calculated coupling constants only on the order of 1 kHz.

We now turn to the discussion of the sign of the χ_{aa} quadrupole coupling constant. Since tha a-axis closely parallels th DO-bond, the positive sign may be surprising at first sight: a negative point charge, positioned at the center of the O-D-bond, which might be expected to present a reasonable, albeit rough, first approximation to the bond, would lead to a negative sign. A closer look however shows that the positive sign is due to the increased *lateral* electron density, which essentially results from the overlap of the deuterium s-orbital(s) with the valence orbitals centered at the neighbouring oxygen atom. The contribution of the increased lateral electron density by far outweighs the contribution from the increased electron density in bond direction. (Note that a shift of electron density outside a plane perpendicular to the bond and running through the D nucleus to positions at the same absolute values for the coordinates with respect to the D-nucleus, but with opposite sign for the relative coordinate in direction of the bond, would leave its contribution to χ_{bond} unchanged).

On the other hand, the effect of the addition of p-type orbitals to the basis at D, which, roughly speaking, allows for partial sp-hybridization in bond direction at the D-nucleus and thus leads to an additional increase of the calculated electron density in the bonding region, is quite in agreement with the above model of a negative point charge in bond direction (closely corresponding to the a-direction). The availability of p-type GTOs lets χ_{bond} go negative by roughly 15% of its value as calculated if only s-type GTOs, as in the case of the GAUSSIAN 6-311G basis, were available at D.

Since correlation tends to reduce the electron charge density in the regions of highest density most, this increase of calculated electron density associated with polarization is partly compensated again in the MP2-calculations. For instance all MP2-results for χ_{aa} are systematically 10 to 13 kHz more positive than the corresponding SCF-results. Finally we note that addition of further GTOs at D, with exponents larger (smaller) by a factor of three than the limiting values reported in the Appendix, changed the calculated coupling constants by less than .5 kHz.

At least part of the remaining difference between the experimental and the calculated values is caused by the neglection of vibrational corrections. In view of the fair success of the Huber-Gerber equation (see

above) we have calculated approximate values for these corrections as follows. We assumed the validity of (8) and cylindrical symmetry of the χ-tensor around the bond axis. Within this approximation the χ-tensor elements are given by

$$\langle|\chi_{aa}|\rangle = \langle|\frac{1}{2}\chi_{\text{Huber}}(r)[3\cos^2(\angle_{(a,\text{OD})}) - 1]|\rangle, \quad (11)$$

$$\langle|\chi_{bb}|\rangle = \langle|\frac{1}{2}\chi_{\text{Huber}}(r)[3\cos^2(\angle_{(b,\text{OD})}) - 1]|\rangle, \quad (12)$$

$$\langle|\chi_{cc}|\rangle = \langle|\frac{1}{2}\chi_{\text{Huber}}(r)[3\cos^2(<_{(c,\text{OD})}) - 1]|\rangle. \quad (13)$$

Here $\langle|\,|\rangle$ denotes vibrational ground state expectation values, $r = r_{(\text{OD})}$ designates the OD-bond length, and $<_{(a,\text{OD})}$ etc. denote the angles between the principal inertia axes and the OD-bond axis. We simplified the vibrational treatment by the assumption of a rigid heavy atom frame and by the additional assumption that the isolated vibration of the deuterium may be treated as separable into a stretching, bending, and torsion with the corresponding wave functions derivable from the following approximate Schrödinger-Equations:

- Stretching:

$$-\frac{\hbar^2}{2m}\left(\frac{\partial^2\psi_s(r)}{\partial r^2}\right) + V_s(r)\cdot\psi_s(r) = E_s\psi_s(r), \quad (14)$$

- Bending ($\delta = <_{(\text{C-O-D})}$ bond angle):

$$-\frac{\hbar^2}{2mr_{\text{eq}}^2}\left(\frac{\partial^2\psi_b(\delta)}{\partial\delta^2}\right) + V_b(\delta)\psi_b(\delta) = E_b\psi_b(\delta) \quad (15)$$

- Torsion ($\tau = \angle_{(\text{D-O-C=O})}$ dihedral (torsional) angle):

$$-\frac{\hbar^2}{2m(r_{\text{eq}}\sin(\delta_{\text{eq}}))^2}\cdot\left(\frac{\partial^2\psi_t(\tau)}{\partial\tau^2}\right) + V_t(\tau)\psi_t(\tau) \quad (16)$$
$$= E_t\psi_t(\tau).$$

As potential functions we have used Morse-approximations for the stretching, $V_s(r)$, and bending potential, $V_b(\delta)$, and a cosine expansion for the torsional potential, $V_t(\tau) = \sum_{n=0}^{8} a_n\cos(n\tau)$. These were adapted to a grid of single point MP2/6-311++G** energies.

The three vibrational Schrödinger-Equations were then solved numerically by the Numerov-Cooley [40 - 42] method and, finally, the effective coupling constants were calculated according to (11) through (13) as

$$\chi_{gg,\text{eff}} = \frac{1}{2}\langle\psi_s|\chi_{\text{Huber}}(r)|\psi_s\rangle \quad (17)$$
$$\cdot\,[3\langle\psi_t\psi_b|\cos^2(\angle_{(g,\text{OD})})|\psi_b\psi_t\rangle - 1]$$

(with $g = a, b, c$ and the proper dependence of the $\angle_{(g,\text{OD})}$-angles on δ and τ).

It turned out that the effect of the anharmonicity in the stretching potential and the pronounced nonlinearity of $\chi_{\text{Huber}}(r)$ with its sharp rise towards smaller r-values largely compensate. Thus the vibrational corrections

$$\Delta\chi_{gg} = \chi_{gg,\text{eff}} - \chi_{gg,\text{eq}} \quad (18)$$

are essentially determined by the effect of orientational averaging. This will also hold for more sophisticated general treatments of the vibrational corrections.

Our final results, including the approximate vibrational corrections obtained within this rigid-frame / local-mode approach are presented in the two rows at the bottom of Table 11. Appearently reasonable vibrational corrections to ab initio deuterium quadrupole coupling constants can be calculated with moderate effort by using Huber's equation for the bond-length dependence of χ_{bond}.

4. Conclusions

With CF_3COOH as an example we have demonstrated that MBFTMW spectroscopy is now capable to supply sufficient and highly accurate data also on the isotopomers in a sample of natural composition to determine the structure of molecules. The combination with quantum chemical calculations provides a great help in the assignment of the spectra of rare isotopomers, measured in natural abundance. Furthermore it complements the determination of the structure, especially in cases where certain isotopomers do not exist, as here in the case of fluorine.

In this way, a fundamental task of rotational spectroscopy can now be solved without difficult and sometimes expansive chemical preparations.

Table 12. Gaussian exponents for the s-, p- and d-type gaussians at hydrogen (deuterium) from Huzinaga's work [37]. The notation is as used in the GAUSSIAN program package [9].

H 0			
S 1 1.0			
68.1600000	1.000000		
S 1 1.0			
10.246500	1.000000		
SPD 1 1.0			
2.3464800	1.000000	1.000000	1.000000
SPD 1 1.0			
0.6733200	1.000000	1.000000	1.000000
SPD 1 1.0			
0.2246600	1.000000	1.000000	1.000000
SPD 1 1.0			
0.0822170	1.000000	1.000000	1.000000

Finally, the fact that lateral overlap of s-type orbitals centered at a quadrupole nucleus with valence orbitals centered at the adjacent nucleus (here O), leads to considerable s-orbital connected contributions to the field gradient at the quadrupole nucleus indicates that earlier discussions of experimental quadrupole coupling constants within the Townes-Dailey model, i.e. in terms of p-orbital populations only, may need revisions.

Acknowledgement

The authors from Kiel thank the other members of the group and Prof. Dr. H. D. Rudolph, Ulm, for fruitful discussions. D. H. S. gratefully acknowledges many fruitful contacts with quantum chemists Dr. U. Fleischer (Bochum), Prof. R. Jaquet (Siegen), and Dr. K. Ruud (Oslo). Funding by Deutsche Forschungsgemeinschaft, Fonds der Chemischen Industrie, and by the Land Schleswig-Holstein is gratefully acknowledged. The authors from Valladolid thank the Direccion General de Investigacion Cientifica y Tecnica (DGICYT, grant PB96-0366) and Junta de Castilla y Leon (grant VA51/96) for financial support. S. A. gratefully acknowledges a FPI grant from the Ministerio de Education y Cultura.

[1] C. C. Costain and G. P. Srivastava, J. Chem. Phys. **35**, 1903 1961).

[2] C. C. Costain and G. P. Srivastava, J. Chem. Phys. **41**, 1620 (1964).

[3] E. M. Bellot jr. and E. Bright Wilson, Tetrahedron **31**, 2896 (1975).

[4] L. Martinache, W. Kresa, M. Wegener, U. Vonmont, and A. Bauder, Chem. Physics **148**, 129 (1990).

Table 13. Extended basis sets as developed by Ahlrichs and coworkers [38], as were used at O, C, and F in addition to the standard basis sets supplied with the GAUSSIAN program package.

C 0 (TZVP)		O 0 (TZV2P)		F 0 (TZVP)	
S 6 1.0		S 6 1.0		S 6 1.0	
13575.3496820	0.000222458	27032.3826310	0.000217263	35479.1004410	0.000215450
2035.2333680	0.001723274	4052.3871392	0.001683866	5318.4728983	0.001670069
463.2256236	0.008925572	922.3272271	0.008739562	1210.4810975	0.008673321
131.2001960	0.035727985	261.2407099	0.035239969	342.8551814	0.035049933
42.8530159	0.110762599	85.3546414	0.111535191	112.0194318	0.111653201
15.5841858	0.242956276	31.0350352	0.255889540	40.7147402	0.259885066
S 2 1.0		S 2 1.0		S 2 1.0	
6.2067139	0.414402634	12.2608607	0.397687309	16.0396781	0.394229669
2.5764897	0.237449687	4.9987076	0.246278494	6.5038187	0.249982386
S 1 1.0		S 1 1.0	S 1 1.0		
0.5769634	1.000000000	1.1703108	1.000000000	1.5440478	1.000000000
S 1 1.0		S 1 1.0		S 1 1.0	
0.2297283	1.000000000	0.4647474	1.000000000	0.6122345	1.000000000
S 1 1.0		S 1 1.0		S 1 1.0	
0.0951644	1.000000000	0.1850454	1.000000000	0.2402798	1.000000000
P 4 1.0		P 4 1.0		P 4 1.0	
34.6972322	0.005333366	63.2749548	0.006068510	80.2339005	0.006368600
7.9582623	0.035864109	14.6270494	0.041912576	18.5940107	0.044303144
2.3780827	0.142158733	4.4501223	0.161538411	5.6867903	0.168672487
0.8143321	0.342704718	1.5275800	0.357069513	1.9511006	0.361663463
P 1 1.0		P 1 1.0		P 1 1.0	
0.2888755	1.000000000	0.5293512	1.000000000	0.6697021	1.000000000
P 1 1.0		P 1 1.0		P 1 1.0	
0.1005682	1.000000000	0.1747842	1.000000000	0.2165130	1.000000000
D 1 1.0		D 1 1.0		D 1 1.0	
0.8000000	1.000000000	0.6900000	1.000000000	1.4000000	1.000000000
		D 1 1.0			
		2.0800000	1.000000000		

Appendix

In the following we present Huzinagas basis [37], which was used at the deuterium nucleus as Table 12 and the TZV2P and TZVP basis sets developed by the Karlsruhe group [38], which were used at the oxygen atoms (TZV2P quality) and carbon and fluorine atoms (TZVP quality) as Table 13. They are given in the notation used in the GAUSSIAN program package, i. e. in the shell definition blocks the first field gives the gaussian exponents and the subsequent field(s) give the contraction coefficient(s). Huzinaga's 6s-basis was used uncontracted. Note further that we have used Huzinaga's exponents for the s-type gaussian functions also for the p-type and d-type functions in order to provide higher flexibility in the immediate neighbourhood of the deuterium nucleus.

[5] S. Antolinez, H. Dreizler, V. Storm, D. H. Sutter, and J. Alonso, Z. Naturforsch. **52a**, 803 (1997).

[6] W. Gordy and R. L. Cook, Microwave Molecular Spectra, John Wiley, New York 1984, Chapt. XIII.

[7] V. M. Stolwijck and B. P. van Eijck, J. Mol. Spectrosc. **113**, 196 (1985).

[8] A. A. J. Maagdenberg, J. Mol. Struct. **41**, 61 (1977).

[9] Gaussian 94, Revision C.3, M. J. Frisch, G. W. Trucks, H. B. Schlegel, P. M. W. Gill, B. G. Johnson, M. A. Robb, J. R. Cheeseman, T. Keith, G. A. Petersson, J. A. Montgomery, K. Raghavachari, M. A. Al-Laham, V. G. Zakrzewski, J. V. Ortiz, J. B. Foresman, J. Cioslowski, B. B. Stefanov, A. Nanayakkara, M. Challacombe, C. Y. Peng, P. Y. Ayala, W. Chen, M. W. Wong, J. L. Andres, E. S. Replogle, R. Gomperts, R. L. Martin, D. J. Fox, J. S. Binkley, D. J. Defrees, J. Baker, J. P. Stewart, M. Head-Gordon, C. Gonzalez, and J. A. Pople, Gaussian, Inc., Pittsburgh (PA) 1995.
[10] U. Andresen, H. Dreizler, U. Kretschmer, W. Stahl, and C. Thomsen, Fresenius J. Anal. Chem. **349**, 272 (1994).
[11] J. Alonso, F. Lorenzo, J. C. Lopez, A. Lessari, S. Mata, and H. Dreizler, Chem. Phys. **218**, 267 (1997).
[12] J.-U. Grabow et al. (to be published).
[13] U. Andresen, H. Dreizler, J.-U. Grabow, and W. Stahl, Rev. Sci. Instrum. **61**, 3694 (1990).
[14] O. Böttcher and D. H. Sutter, Z. Naturforsch. **43 a**, 47 (1988), Appendix.
[15] J. Haekel and H. Mäder, Z. Naturforsch. **44 a**, 203 (1988).
[16] W. H. Press, S. A. Teukolsky, W. T. Vetterling, B. P. Flannery, Numerical Recipes; University Press, Cambridge 1992, Chap. 15.
[17] J.-U. Grabow, PhD Thesis, Kiel 1992, Chapt. IV.
[18] W. Gordy and R. L. Cook, Microwave Molecular Spectra, John Wiley, New York 1984, Chapt. VIII.
[19] J. K. G. Watson in J. R. Durig (Ed.), Vibrational Spectra and Structure, Elsevier, Amsterdam 1977, p. 1.
[20] W. Gordy and R. L. Cook, Microwave Molecular Spectra, John Wiley, New York 1984, Chapt. VIII, p. 331.
[21] V. Typke, University of Ulm, Germany, private communication. Compare too: J. Mol. Spectrosc. **63**, 170 (1976).
[22] H. Hartwig and H. Dreizler, Z. Naturforsch. **51a**, 923 (1996).
[23] W. Gordy and R. L. Cook, Microwave Molecular Spectra, John Wiley, New York 1984, Table 8.17.
[24] K.-M. Marstokk and H. Møllendal, Acta Chem. Scand. **52**, 296 (1998).
[25] J. Kraitchman, Amer. J. Phys. **21**, 17 (1953).
[26] C. C. Costain, J. Chem. Phys. **29**, 864 (1958).
[27] H. D. Rudolph, University of Ulm, Germany, private communication.
[28] B. P. van Eijck, J. Mol. Spectr. **91**, 348 (1982).
[29] P. Nösberger, A. Bauder, and Hs. H. Günthard, Chem. Phys. **1**, 418 (1973).
[30] V. Typke, University of Ulm, Germany, private communication.
[31] C. C. Lin and J. D. Swalen, Rev. Mod. Phys. **31**, 841 (1959).
[32] P. Pyykkø, Z. Naturforsch. **47a**, 189 (1992).
[33] S. Gerber and H. Huber, J. Mol. Spectrosc. **134**, 168 (1989).
[34] H. Huber, J. Chem. Phys. **83**, 4591 (1985).
[35] B. P. Dailey and C. H. Townes, J. Chem. Phys. **23**, 118 (1955) and references cited therein.
[36] C. Møller and M. S. Plesset, Phys. Rev. **46** 618 (1934).
[37] S. Huzinaga, J. Chem. Phys. **42**, 1293 (1965), Table V.
[38] A. Schäfer, H. Horn, and R. Ahlrichs J. Chem. Phys. **97**, 2571 (1992).
[39] H. Huber and P. Diehl, Mol. Phys. **54**, 725 (1985).
[40] B. Numerov, Publs. Observatoire Central. Astrophys. Russ. **2**, 188 (1933).
[41] J. W. Cooley, Math. Comp. **15**, 363 (1961).
[42] P. O. Löwdin, J. Mol. Spectrosc. **10**, 12 (1963).